Supplemental Table 1: Intrinsic Immune Genes

Human		
BCL10	GCLC	PARK7
BCL2	GPX1	PIK3CA
BCL2A1	GSTP1	POR
BCL6	GZMB	REL
BIK	HMOX1	RELB
BIRC2	IKBKE	RIPK1
CAT	IL15	RIPK2
CCL13	IL16	RNF31
CCL17	IL18	SOCS3
CCL18	IL1B	SOD1
CCL19	IL1R1	STAT1
CCL2	IL2RA	STAT4
CCL21	IL6	STAT6
CCL22	IRAK1	TLR2
CCL24	IRF1	TNF
CCL26	IRF3	TNFAIP3
CCL27	IRF4	TNFRSF18
CCL5	IRF6	TNFRSF1A
CCR2	IRF8	TNFRSF1B
CCR5	LTBR	TNFSF4
CD40	MAP2K1	
CDKN1A	MAP2K2	
CDKN1B	MAP2K4	
CEBPB	MAP3K14	
CHUK	MAPK1	
CXCL1	MAPK13	
CXCL12	MMP1	
CXCL13	MMP10	
CXCL16	MMP2	
CXCL2	MMP7	
CXCL5	MYC	
CXCL9	NCF1	
CXCR3	NFE2L2	
CYBB	NFKB1	
CYP2A13	NFKB2	
DDX58	NFKBIA	
ELK1	NLRP3	
EPHX1	NOD1	
FAS	NOS3	
FOS	NPM1	
GATA3	NQO1	

Mouse		
BCL10	EPHX1	NLRP3
BCL2	FAS	NOD1
BCL2a1a	FOS	NOS3
BCL2a1b	GATA3	NPM1
BCL2a1d	GCLC	NQO1
BCL6	GPX1	PARK7
BIK	GSTP1	PIK3CA
BIRC2	GZMB	POR
CAT	HMOX1	REL
CCL21	IKBKE	RELB
CCL17	IL15	RIPK1
CCL19	IL16	RIPK2
CCL2	IL18	RNF31
CCL21a	IL1B	SOCS3
CCL22	IL1R1	SOD1
CCL24	IL2RA	STAT1
CCL26	IL6	STAT4
CCL27a	IRAK1	STAT6
CCL3	IRF1	TLR2
CCL5	IRF3	TNF
CCR2	IRF4	TNFAIP3
CCR5	IRF6	TNFRSF18
CD40	IRF8	TNFRSF1A
CDKN1A	JUN	TNFRSF1B
CDKN1B	LTBR	TNFSF4
CEBPB	MAP2K1	
CHUK	MAP2K2	
CXCL1	MAP2K4	
CXCL12	MAP3K14	
CXCL13	MAPK1	
CXCL16	MAPK13	
CXCL2	MMP10	
CXCL5	MMP1a	
CXCL9	MMP2	
CXCR3	MMP7	
CYBB	MYC	
CYP2a12/CYP2a22	NCF1	
CYP2a4	NFE2l2	
CYP2a5/CYP2a21-ps	NFKB1	
DDX58	NFKB2	
ELK1	NFKBIA	

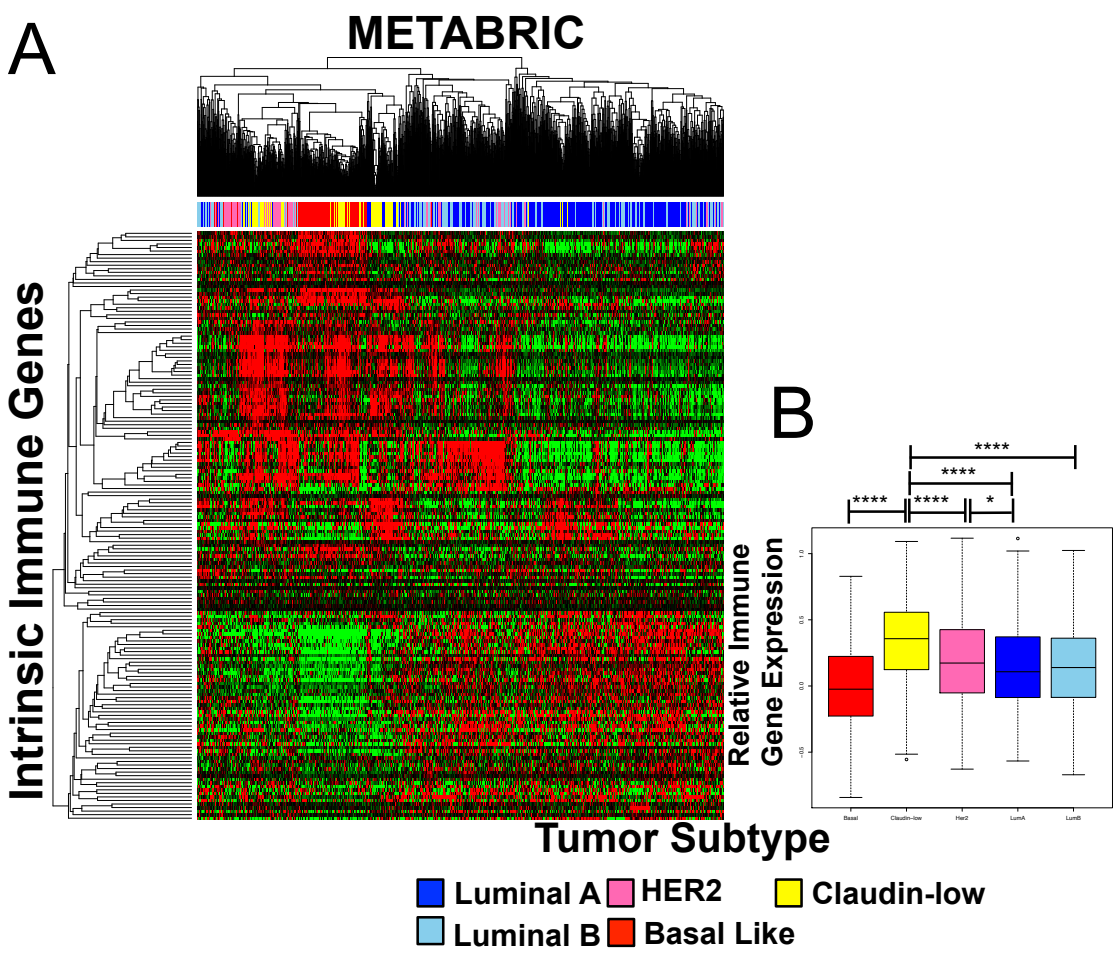

Supplemental Figure S1: Human tumor subtypes exhibit differential immune gene expression. (**A**) Unsupervised hierarchical clustering of breast cancer samples from METABRIC by intrinsic immune gene list. (**B**) Overall expression of the immune gene signature by each subtype. Statistical significance determined by Kruskal-Wallis test, with Dunn's post-test for multiple comparisons (n=1,981). * denotes $p < 0.05$, **** denotes $p < 0.0001$.

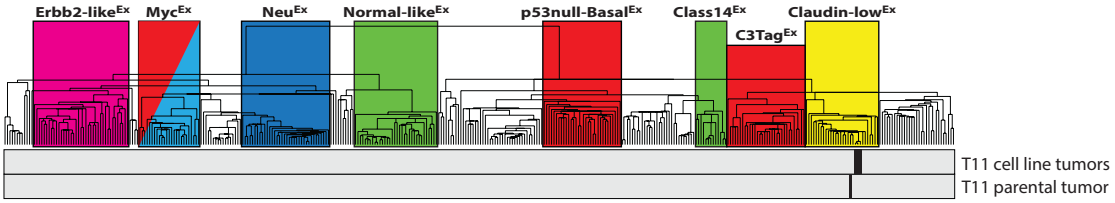

Supplemental Figure S2: Tumors derived from T11 cell line result in true claudin-low tumors. Three T11 cell line-derived tumors were normalized to a 385 microarray dataset consisting of tumors from 27 murine models of breast carcinoma and normal mammary tissue [21]. A supervised cluster using murine intrinsic genes was performed, with the sample dendrogram displayed. The eight murine classes identified as human subtype counterparts are highlighted. The cluster locations of the T11 parental tumor and the three T11 cell line derived tumors, which had a dendrogram correlation of 0.84, are displayed below the dendrogram as black lines.

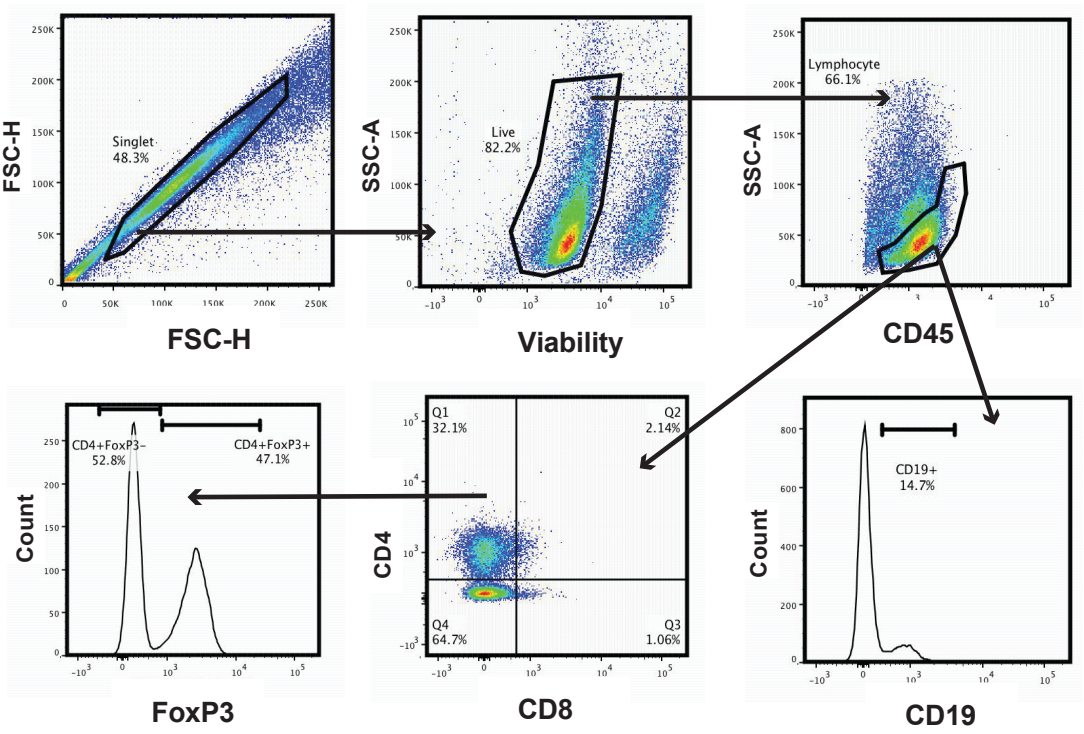

Supplemental Figure S3: Representative FACS analysis diagram. Shown is a representative gating schema for the FACS analysis of tumor-infiltrating lymphocytes from an untreated 20 mm^2 T11 tumor. Following generation of single-cell suspensions from tumor tissue and enrichment for leukocytes by density-gradient centrifugation, samples were analyzed by FACS. Viable $CD45^+$ cells were gated on CD8 and CD19 to enumerate cytotoxic T cells and B cells respectively, and $CD4^+$ cells were analyzed for FoxP3 expression to enumerate helper T cells ($CD4^+FoxP3^-$) and regulatory T cells ($CD4^+FoxP3^+$).

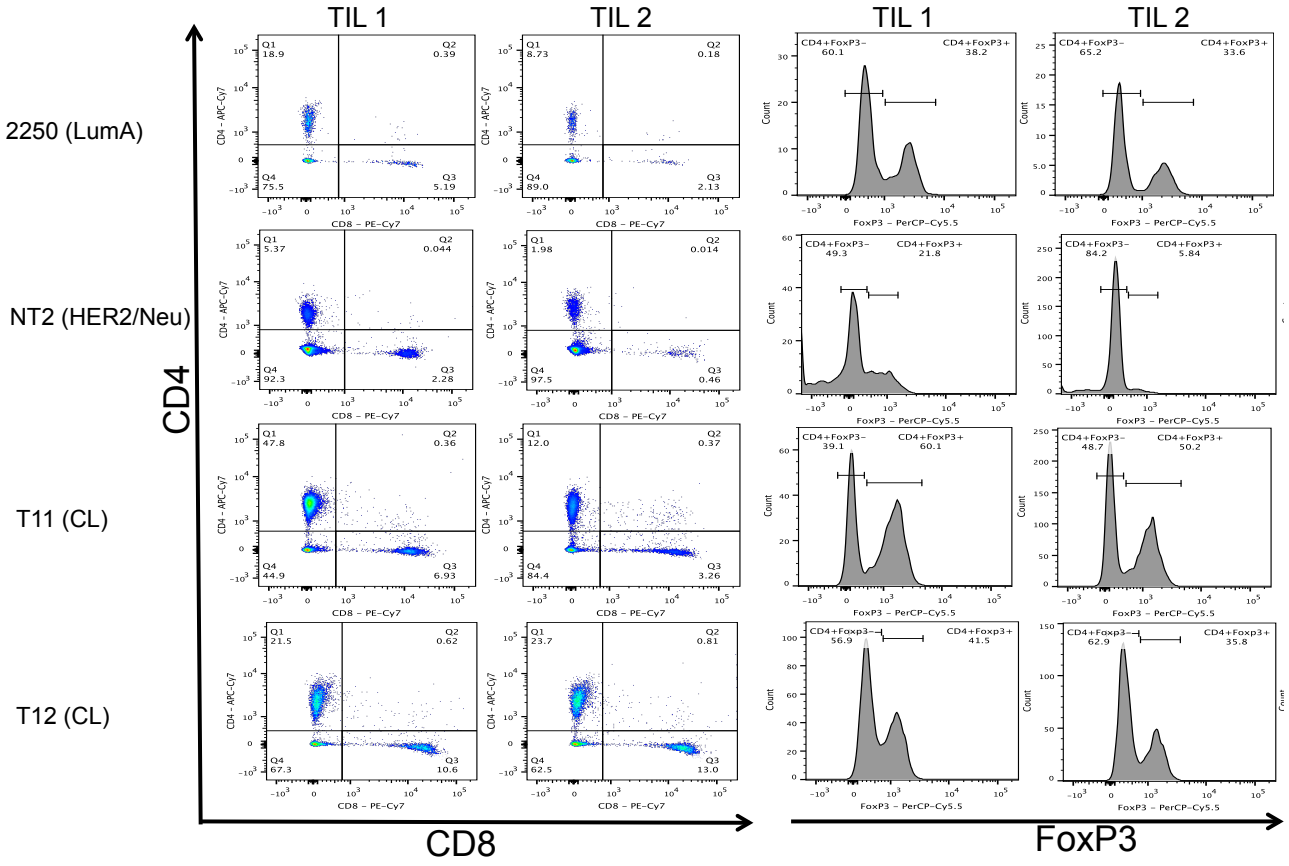

Supplemental Figure S4: Representative FACS plots of tumor infiltrating lymphocytes. WT mice were injected with 1 x 10^6 2250 tumor cells or 1 x 10^4 T11 or T12 cells. Neu-N mice were injected with 5 x 10^4 NT2 cells. Tumors were harvested at 100mm^2 (2250 n=10, NT2 n=5, T11 n=10, T12=6), digested, enriched for lymphocytes, and analyzed by FACS. Data are representative of data presented in Figure 2.

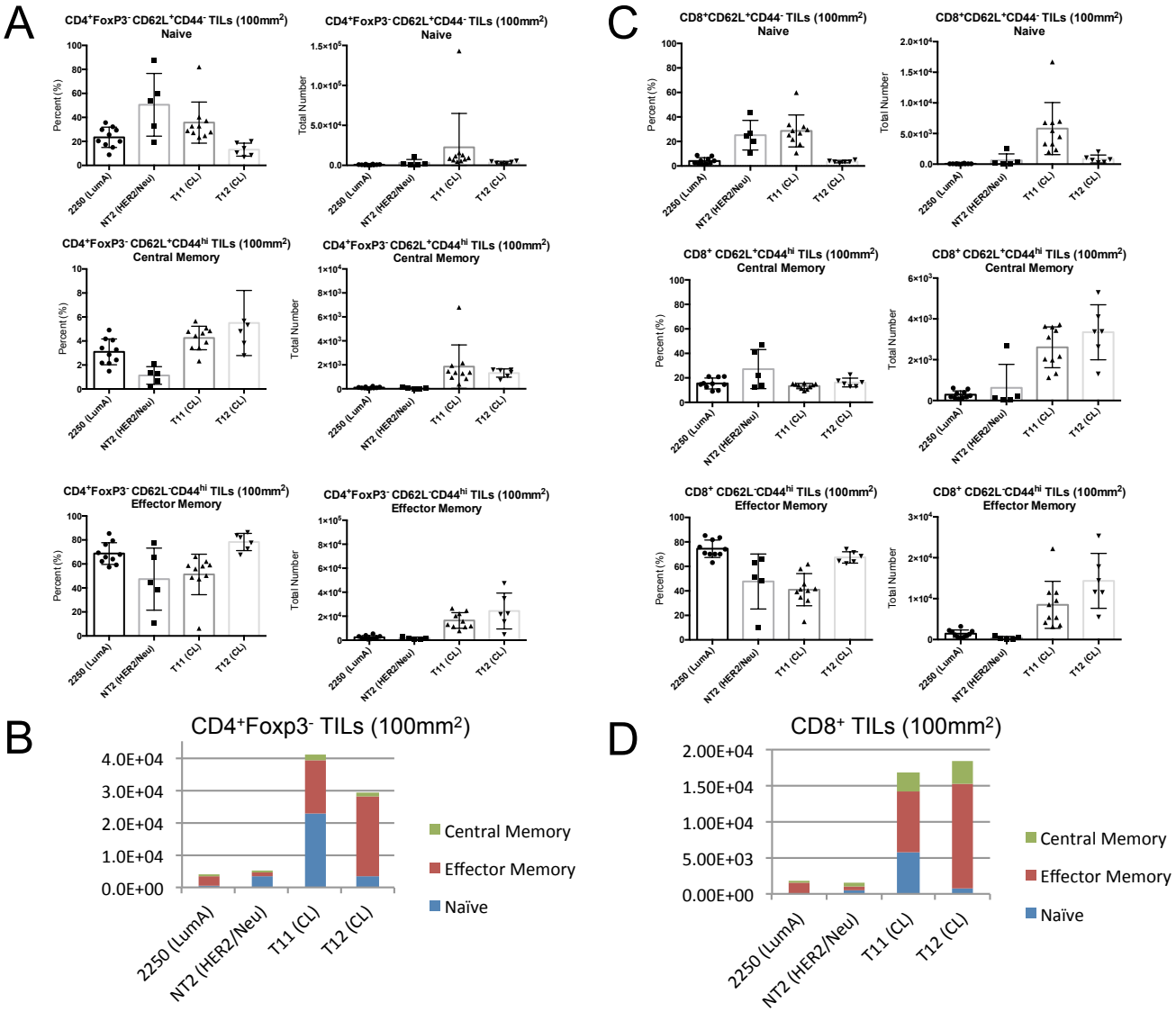

Supplemental Figure S5: CD4$^+$ and CD8$^+$ T cell activation subsets. WT mice were injected with 1 x 10^6 2250 tumor cells or 1 x 10^4 T11 or T12 cells. Neu-N mice were injected with 5 x 10^4 NT2 cells. Tumors were harvested at 100 mm^2 (2250 n=10, NT2 n=5, T11 n=10, T12=6), digested, enriched for lymphocytes, and analyzed by FACS. CD62L$^+$CD44^{lo} T cells are considered naïve; CD62L$^+$CD44^{hi} T cells are considered activated or central memory; and CD62L$^-$ CD44^{hi} T cells are considered effector memory. (**A**) Percent and total number naïve, central memory, and effector memory CD4$^+$Foxp3$^-$ T cells. (**B**) Total number of each cell type from (**A**) graphed as a stacked column bar graph. (**C**) Percent and total number naïve, central memory, and effector memory CD8$^+$ T cells. (**D**) Total number of each cell type from (**C**) graphed as a stacked column bar graph.

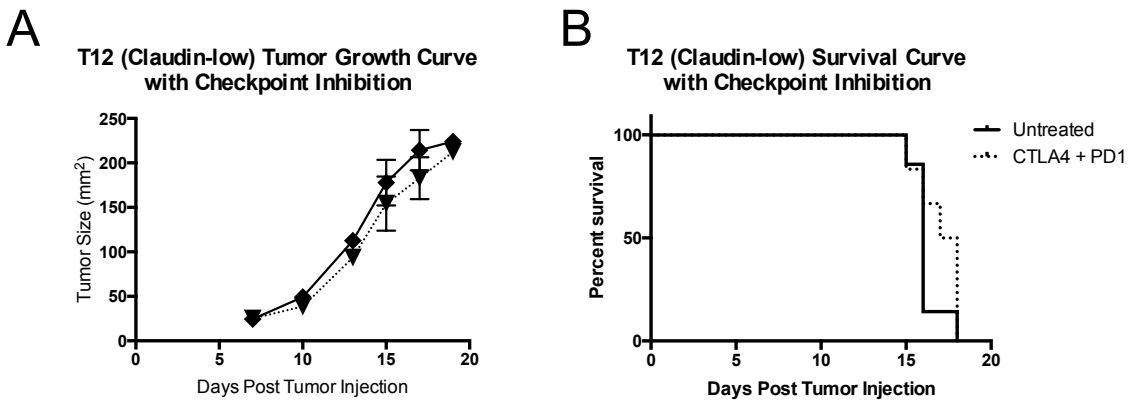

Supplemental Figure S6: PD-1 and CTLA-4 inhibition do not increase survival in T12 claudin-low tumor bearing mice. WT mice were injected in 1 x 10^5 T12 tumor cells. (**A**) Growth curves of T12 tumor bearing mice receiving anti-PD-1 and anti-CTLA-4. (**B**) Survival analysis of data presented in (**A**) (n=6 for each group).

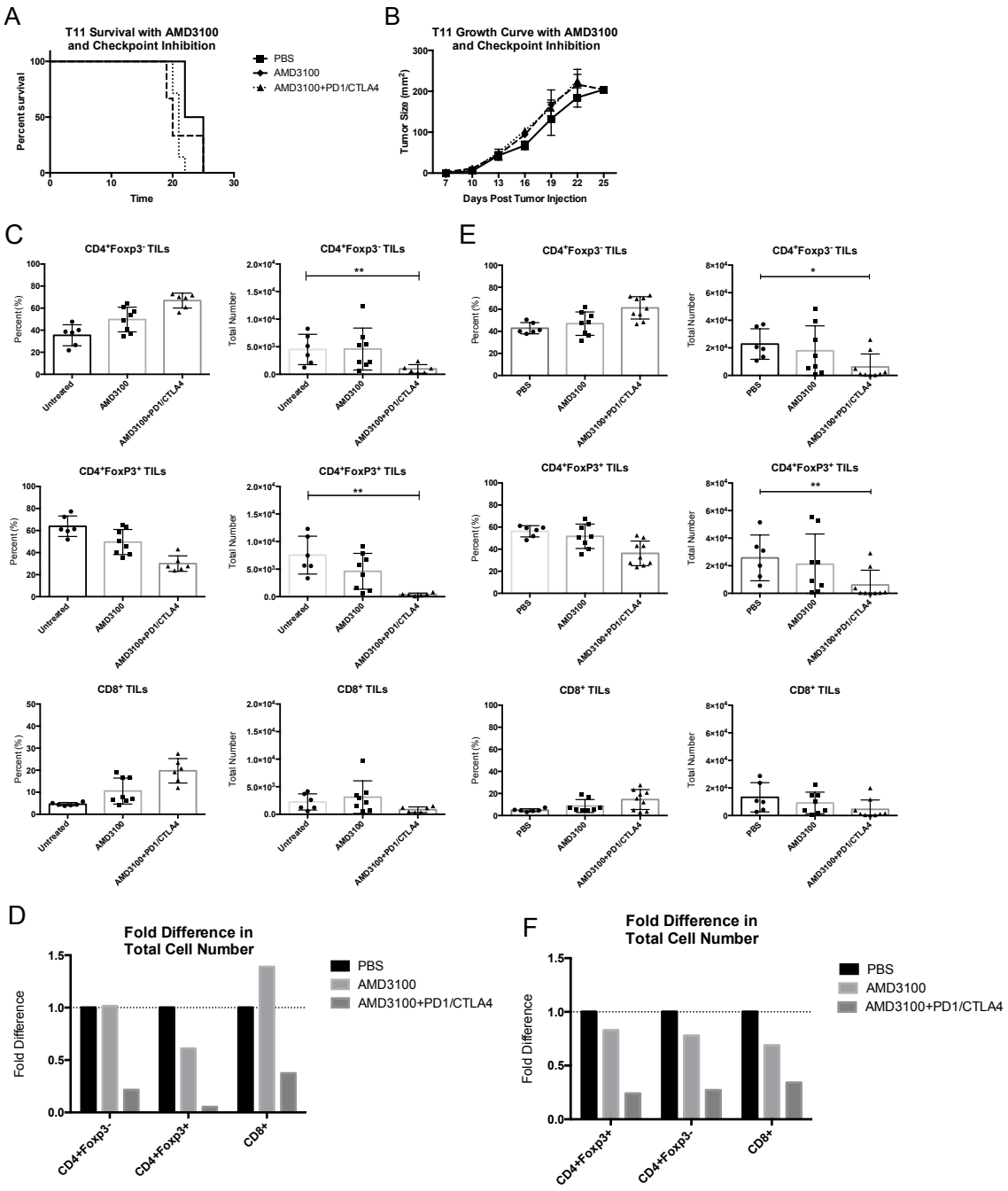

Supplemental Figure S7: CXCR4/CXCL12 blockade does not delay T11 tumor growth or enhance survival. WT mice were implanted on day -2 with osmotic pumps loaded with PBS or 10 mg AMD3100 in PBS (PBS n = 6, AMD3100 n=8, AMD3100+PD1/CTLA4 n=9) and challenged with 1 x 10^4 T11 cells. (**A**) Growth curves of T11 tumor bearing mice receiving AMD3100 with or without anti-PD-1 and anti-CTLA-4. (**B**) Survival analysis of data presented in (**A**). (**C**-**D**)Tumors harvested on day 12 PTI and FACS analyzed. (**C**) Percent and total number of $CD4^+Foxp3^-$, $CD4^+Foxp3^+$, and $CD8^+$ TILs. (**D**) The fold difference in the total number of TILs normalized to PBS group. (**E**-**F**) Tumors harvested on day 16 PTI and FACS analyzed. (**E**) Percent and total number of $CD4^+Foxp3^-$, $CD4^+Foxp3^+$, and $CD8^+$ TILs. (**F**) The fold difference in the total number of TILs normalized to PBS group. Statistical significance determined by Kruskal-Wallis test with Dunn's post-test for multiple comparisons. * denotes $p < 0.05$, ** denotes $p < 0.01$.

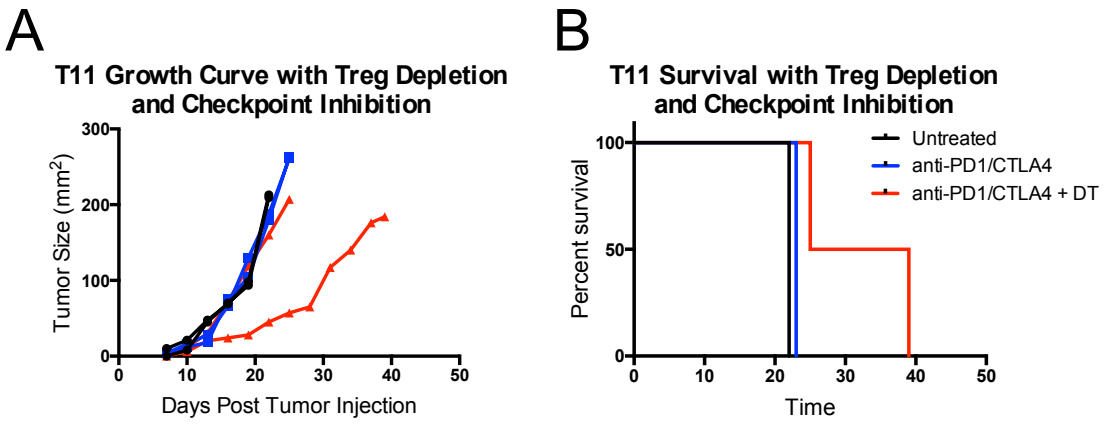

Supplemental Figure S8: Regulatory T cell depletion after tumor establishment with anti-PD-1 and anti-CTLA-4 immune checkpoint inhibition delays T11 tumor growth. WT or FoxP3-DTR mice were injected with 1 x 10^4 T11 cells. DEREG mice received 1µg diphtheria toxin (DT) on day 6, 7, 13, and 14 PTI. DT + PD-1 + CTLA4 mice received 1µg DT on day 6, 7, 13, and 14 PTI, and anti-PD-1 and anti-CTLA4 antibody on day -1 then every other day for the duration of the experiment. (**A**) Individual replicates of tumor growth curves. (**B**) Mice depleted of T_{regs} and receiving anti-PD-1 and anti-CTLA4 (n = 2) have a non-significant survival benefit compared to untreated (n=2) or anti-PD-1 and anti-CTLA4 alone (n = 2).

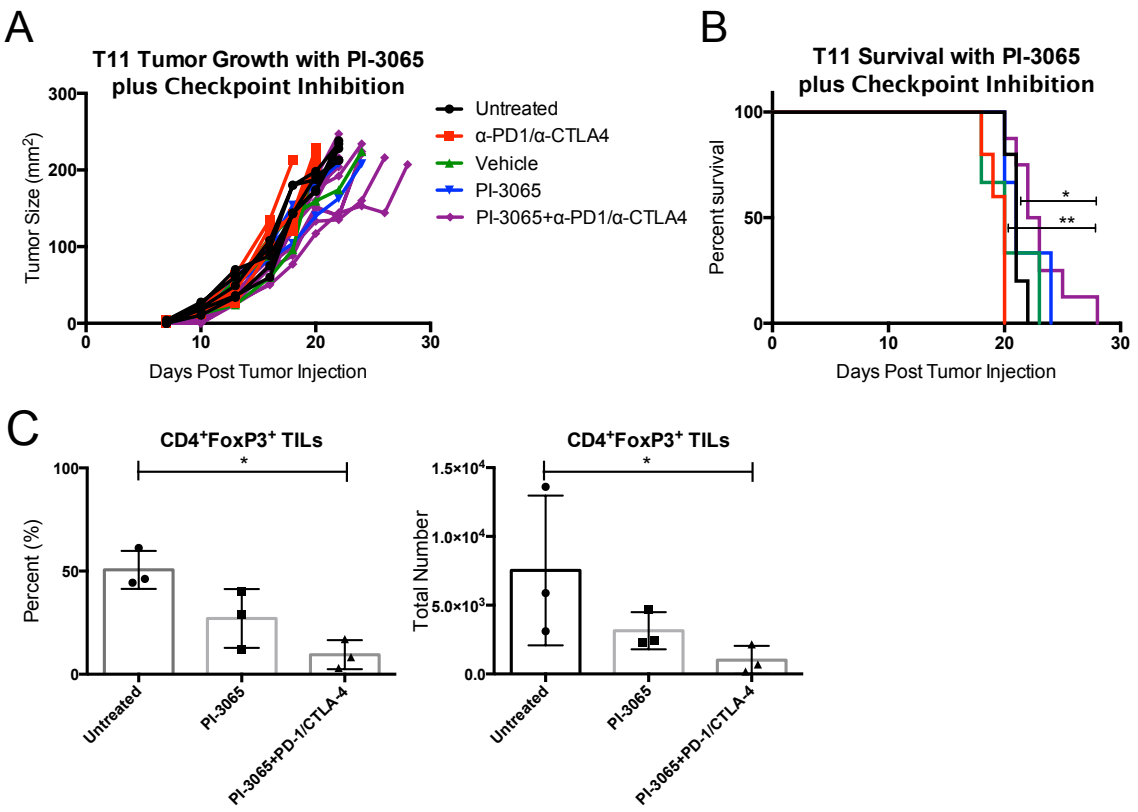

Supplemental Figure S9: Selective inhibition of PI3K family member p110δ by PI-3065 combined with checkpoint inhibition slightly delays T11 tumor growth and improves survival. WT mice were injected with 1 x 10^4 T11 cells. Mice receiving PI-3065 or vehicle were given 75mg/kg of PI-3065 or vehicle only daily by oral gavage. Anti-PD1 + anti-CTLA4 mice received anti-PD1 and anti-CTLA4 antibody on day -1 then every other day for the duration of the experiment. (**A**) Individual replicates of tumor growth curves. (**B**) Mice receiving PI-3065 anti-PD1 and anti-CTLA4 (n = 8) have a significant survival benefit compared to untreated (n=5) and anti-PD1 and anti-CTLA4 alone (n = 5) (untreated vs. PI-3065 + anti-PD1/CTLA4: p=0.0415, anti-PD1/CTLA4 vs PI-3065 + anti-PD1/CTLA4): p = 0.0015. Statistical significance of survival determined by log-rank test. (**C**) Percent and total number $CD4^+FoxP3^+$ T_{regs} isolated from the tumor at day 18 PTI in untreated mice (n=3) compared to mice treated with PI-3065 alone (n=3) or PI-3065 plus anti-PD-1 and anti-CTLA4 (n=3). Statistical significance determined by Kruskal-Wallis test with Dunn's post-test for multiple comparisons. * denotes $p < 0.05$.